SAND97-1118C
CONF-970231--34

Incorporating many-body effects into modeling of semiconductor lasers and amplifiers

C.Z. Ning[a], R.A. Indik[a], J.V. Moloney[a], W.W. Chow[b], A. Girndt[c], S.W. Koch[c], and R. Binder[d]

[a] Arizona Center for Mathematical Sciences, University of Arizona, Tucson, AZ 85721

[b]Sandia National Laboratories, Albuquerque, NM 87185

[c] Fachbereich Physik, Universität Marburg, D-35032 Marburg, Germany

[d] Optical Sciences Center, University of Arizona, Tucson, AZ 85721

ABSTRACT

Major many-body effects that are important for semiconductor laser modeling are summarized. We adopt a bottom-up approach to incorporate these many-body effects into a model for semiconductor lasers and amplifiers. The optical susceptibility function (χ) computed from the semiconductor Bloch equations (SBEs) is approximated by a single Lorentzian, or a superposition of a few Lorentzians in the frequency domain. Our approach leads to a set of effective Bloch equations (EBEs). We compare this approach with the full microscopic SBEs for the case of pulse propagation. Good agreement between the two is obtained for pulse widths longer than tens of picoseconds.

Keywords: Many-body interactions, simulation and modeling, semiconductor lasers, gain and refractive index dispersions

1. INTRODUCTION

Many-body effects in semiconductors have been mostly studied for ultra-short pulse propagation[1,3–6] and for the gain and refractive index computation.[2] As a results of these studies, the microscopic theory known as the semiconductor Bloch equations (SBEs) is now quite well established. This is achieved through systematic comparison of the gain and refractive index measurements with theoretical computation,[6–10] or through comparing pulse reshaping in pump-probe experiments with theoretical prediction. Although the theory itself is still a topic of current research activity and more systematic comparison with experiments of various kinds is still necessary, we think that the theory now should be applied in a systematic way to modeling and simulation of space-time dynamics of semiconductor lasers on nano- to tens of pico-second time scales.

In this paper, we first summarize the major many-body effects that are relevant to semiconductor laser modeling. We will show why the conventional approach to semiconductor laser modeling based on the rate-equation apprximation is not adequate. A procedure will then be introduced that takes into account the full gain nonlinearity and dispersion of gain and refractive index, computed using the microscopic many-body theory. This approach leads to a set of effective equations similar to the Bloch equations for two level atoms, thus the term effective Bloch equations (EBEs). A comparison of the EBEs with the semiconductor Bloch equations for the pulse propagation is made to demonstrate the validity and limitation of the model.

2. MANY-BODY EFFECTS

The free-carrier version of the microscopic theory for semiconductor lasers was first formulated about thirty years ago.[11–13] Although some of the many-body effects in semiconductors became known in 1970's,[14] a systematic theory for semiconductor-light interactions including Coulomb interactions was only available much later.[15,16,1,2] The many-body version of the microscopic theory is very often presented in the form of the semiconductor Bloch equations.[15,1,2]

C.Z.N.:cning@acms.arizona.edu
R.A.I.:indik@acms.arizona.edu
J.V.M.:jml@acms.arizona.edu
W.W.C.:wwchow@somnet.sandia.gov
A.G.:girndt@ax1311.physik.uni-marburg.de
S.W.K.: koch@ax1311.physik.uni-marburg.de
R.B.:binder@argonaut.opt-sci.arizona.edu

2.1. The semiconductor Bloch equations (SBEs)

Under the slowly varying envelope (SVE) and rotating wave approximation (RWA), the interaction of a semiconductor with a laser field can be described by the following set of equations[1,15,2]:

$$\frac{\partial E}{\partial z}+\frac{n_g}{c}\frac{\partial E}{\partial t} = \frac{iK\Gamma}{2\epsilon_0\epsilon_b}\frac{1}{V}\sum_k \mu_k p_k \tag{1}$$

$$\begin{aligned}\frac{\partial p_k}{\partial t} &= -\left[\Gamma_{out}(k)-i\delta_k\right]p_k+\frac{i\mu_k}{\hbar}E(n_{e,k}+n_{h,k}-1)\\ &+ \sum_{k'\neq k}\left[-\frac{i}{\hbar}(n_{e,k}+n_{h,k}-1)V_{s,k,k'}+\Gamma_{in}(k',k)\right]p_{k'}\end{aligned} \tag{2}$$

$$\begin{aligned}\frac{\partial n_{\alpha,k}}{\partial t} &= \frac{i}{\hbar}\left[\mu_k E p_k^*-\mu_k^* E^* p_k\right]+\left.\frac{\partial n_{\alpha,k}}{\partial t}\right|_{pump}\\ &+ \frac{i}{\hbar}\sum_{k'\neq k}V_{s,k,k'}\left[p_{k'}p_k^*-p_{k'}^*p_k\right]+\left.\frac{\partial n_{\alpha,k}}{\partial t}\right|_s,\quad(\alpha=e,h),\end{aligned} \tag{3}$$

where E is the complex field amplitude written with respect to a reference frequency ω_c. $K=\frac{\omega_c}{c}n_b$ is the wave vector in the background medium. Γ is the confinement factor. The n_g and $n_b=\sqrt{\epsilon_b}$ are the group index and phase index. The other constants have the usual meanings. The last two equations for the interband polarization (p_k), electron ($n_{e,k}$) and hole ($n_{h,k}$) populations are derived up to the second order in the screened Coulomb potential $V_{s,k,k'}$. The $\delta_k=\omega_c-\omega_k$ is the detuning between the individual transition frequency ω_k and the reference frequency of E. $\Gamma_{out}(k)$ and $\Gamma_{in}(k,k')$ are scattering rates out of, and into, the state k, respectively, which are both second order in the screened Coulomb potential and both functions of the Fermi distributions for electrons ($f_{e,k}$) and for holes ($f_{h,k}$). When more than one conduction or valence band is involved, the corresponding equations for the distribution functions ($n_{e,k}$ or $n_{h,k}$) should be added and similar polarization equation should be written for each transition channel.

To obtain the optical susceptibility function, we solve(2) in the Fourier representation. We assume that the actual distributions $n_{e,k}$ and $n_{h,k}$ can be approximated by the corresponding Fermi-Dirac distributions $f_{e,k}$ and $f_{h,k}$, respectively. We further assume that the explicit time dependence of total carrier density can be ignored when performing the Fourier transformation. Using the Fourier space definition of the susceptibility function $\chi(\omega,N)$, $\tilde{p}_k(\omega)=\epsilon_0\epsilon_b\chi_k(\omega,N)\tilde{E}(\omega)$ (quantities with tilde represent their Fourier transforms), we obtain from (2)

$$\begin{aligned}\left[-i(\delta_k+\omega)+\Gamma_{out}(k)\right]\chi_k &= \frac{i\mu_k}{\hbar\epsilon_0\epsilon_b}(f_{e,k}+f_{h,k}-1)\\ &+ \sum_{k'\neq k}\{-\frac{i}{\hbar}(f_{e,k}+f_{h,k}-1)V_{s,k,k'}+\Gamma_{in}(k',k)\}\chi_{k'},\end{aligned} \tag{4}$$

We see that, because of the non-diagonal terms in the second line, the above equation cannot be solved in a closed form. In general, this integral equation has to be solved numerically. We note that, however, since equation (2) is accurate up to second order, we need only to solve equation (4) iteratively up to the second order in Coulomb potential. This leads to the following expression:

$$\begin{aligned}\chi_k &= \chi_k^0\left(1+\sum_{k'}\left[\frac{1}{\mu_k}V_{s,k,k'}+\frac{1}{\mu_k}\sum_{k_1}V_{s,k,k_1}\chi_{k_1}^0\frac{1}{\mu_{k_1}}V_{s,k_1,k'}+\frac{1}{\Lambda_k\chi_k^0}\Gamma_{in}(k,k')\right]\chi_{k'}^0+\ldots\right)\\ &\equiv \chi_k^0\mathcal{Q}_k\end{aligned} \tag{5}$$

where the $\mathcal{Q}_k$ is the new enhancement factor due to the Coulomb interaction and can be approximated by

$$\mathcal{Q}_k^{-1} = 1 - \sum_{k'} \left[\frac{1}{\mu_k} V_{s,k,k'} + \frac{1}{\Lambda_k \chi_k^0} \Gamma_{in}(k,k') \chi_{k'}^0 \right], \tag{6}$$

where Λ_k and χ_k^0 are given respectively by

$$\Lambda_k = -i(\delta_k + \omega) + \Gamma_{out}(k), \tag{7}$$

$$\chi_k^0 = \frac{i\mu_k(1 - f_{e,k} - f_{h,k})}{\hbar\epsilon_0\epsilon_b\Lambda_k}. \tag{8}$$

The χ_l^0 is the free-carrier susceptibility with a k and carrier density dependent dephasing rate $\Gamma_{out}(k)$.

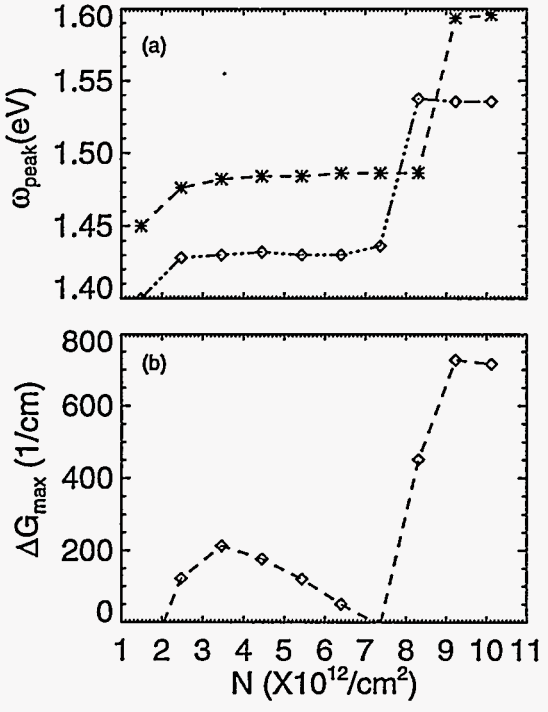

Figure 1. (a) Peak gain frequency vs. carrier density for the free-carrier model (stars) and for the many-body model (diamonds). (b) Peak gain difference between the many-body model and free-carrier model (with bandgap renormalization included).

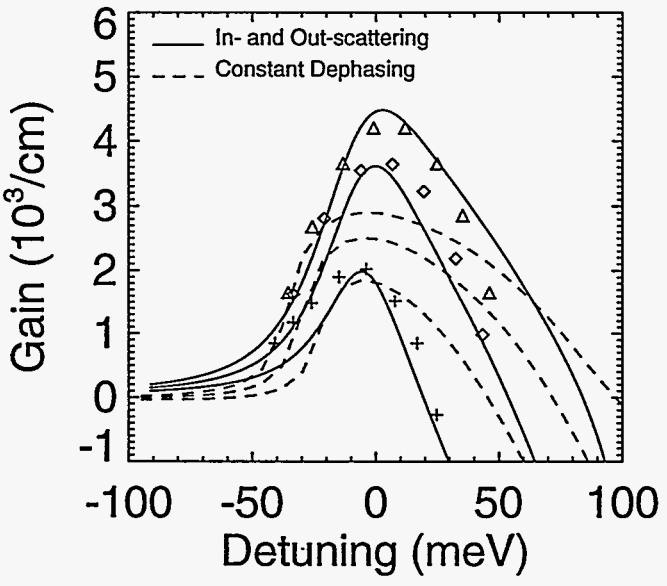

Figure 2. Gain spectra for a 10 nm InGaAs quantum well. Dashed lines represent many-body gain with a constant dephasing rate. Solid line represent many-body gain model with in- and out-scattering terms. The symbols (crosses, diamonds, and triangles) represent experimentally measured gain by Bossert and Gallant[21].

The Coulomb enhancement factor $\mathcal{Q}_k$ is analogous to the one used in[1,2] without the Γ_{in} term. The validity of this approximation and its accuracy should be checked against experimental measurements of the gain and refractive index change.

2.2. Bandgap renormalization

From the above discussion, we can immediately identify several effects of the many-body interactions: First the individual transition frequency ω_k is renormalized by the Coulomb interaction[2]

$$\hbar\omega_k = E_{g,0} + E_{e,k} + E_{h,k} + \Delta E(N), \tag{9}$$

where $E_{g,0}$, $E_{e,k}$, and $E_{h,k}$ are the bare band gap, electron and hole kinetic energies, respectively. The last term is the bandgap shrinkage due to the Coulomb interaction which is treated usually to first order in the Coulomb potential. This term depends on the total carrier density N. As a result, the gain spectrum is shifted toward the red. This fact is shown in Fig.1(a) where the peak gain frequency is plotted against the carrier density for the cases with (diamonds) and without (stars) many-body interactions. The structure considered here is a 10 nm GaAs quantum well with $Al_{0.35}Ga_{0.65}As$ confining layers on both sides. In Fig.1(a) we see that the peak gain frequency is shifted toward red by about 50 meV with respect to the free-carrier gain model due to the bandgap renormalization. It is to be noted that the actual band gap renormalization is usually larger than this number. With the increase of carrier density, there are two things happening at the same time. One is the red shift of the band edge, and another is the blue shift of the gain peak. The final peak gain position reflects the balance of the two. This peak gain shift (about 10 ThZ) is important for predicting laser frequency, because the typical laser intermode spacing is much smaller than this value.

2.3. Coulomb enhancement

Because of the interband Coulomb attraction between electrons and holes, the transition dipole moment is enhanced. This is the Coulomb enhancement factor represented by (6). In Fig.1(b) we show the peak gain difference (denoted by ΔG_{max}) between the cases with and without Coulomb enhancement effect. A positive ΔG_{max} means that peak gain with Coulomb enhancement is larger. We see that ΔG_{max} increases initially with density increase until a maximum is reached. Afterwards ΔG_{max} decreases to zero with further density increase. This behavior can be understood in the following way. We expect the Coulomb interaction to increase with increase of the average interparticle distance. With further increase of the carrier density, the screening becomes important, which decreases the effective interactions. In the large density limit, the strong screening leads to a free gas-like situation, except for an overall bandedge shift. We therefore should expect the agreement of the peak gain for the cases with and without Coulomb enhancement in the limit of large density. A similar process repeats itself for the second quantized band, as is evidenced by the peak frequency jumps in Fig.1(a) and the ΔG_{max} rise at density around $7.5 \times 10^{12} cm^{-2}$. At the density value of $3.5 \times 10^{12} cm^{-1}$, where the ΔG_{max} peaks at about 200 cm^{-1}, the absolute gain is about 1100 cm^{-1}. The relative gain difference between the case with and without Coulomb enhancement is between 15 to 20 percent. This difference should be quite important for laser operation.

2.4. The line shape of the gain spectrum

Although line shape is one of the most important issues for semiconductors, semiconductor gain and refractive index have almost exclusively been computed using a simple Lorentzian line with the line width constant for all k-vectors (see, however[26] for examples of exceptions). Only very recently has a detailed computation been performed with both in and out-scattering terms[32,5] included, as represented by Γ_{in} and Γ_{out} in (2). The inclusion of both in- and out-scattering may help resolve a serious difference on the shape of the gain spectrum between experiment and a theory that uses a simple constant Lorentzian line width. The issue concerns the gain rise at the bare bandedge. While theoretical calculation gives a very sharp increase of gain at the bandedge, experiments give a consistently much smoother rise.[21–23] This difference was emphasized by Hybertsen et al. recently.[22] Fig. 2 shows a comparison of gain spectra at three densities with a constant Lorentzian line width of 10^{13} s^{-1} (dashed lines) and those calculated with a model including both in- and out-scattering terms. As is clearly shown there, even in the frequency domain near the gain peak, the two theories give drastically different results. The experimental results[21] are also included, as marked with different symbols. Clearly the theory with both in- and out scattering gives much better agreement. This comparison therefore leads us to believe that the consistent difference of the gain spectra at band edge between experiment and theory is due to the inappropriate treatment of the scattering terms.

3. THE CONVENTIONAL SEMICONDUCTOR LASER MODELING

3.1. Rate equations with linearized gain

Contrary to the detailed microscopic theory represented by the SBEs, semiconductor lasers are usually modeled with a much simpler model,[25,27,28] with all, or most of the above many-body effects ignored. The essence of this type

of modeling is the equations for E and the total carrier density $N = \frac{1}{V}\sum_k n_{\alpha,k}$.[2,27] By adiabatically eliminating p_k (setting $\dot{p}_k = 0$) in (2), one obtains a static susceptibility function through $P = \frac{1}{V}\sum_k \mu_k p_k \equiv \epsilon_0 \epsilon_b \chi(N) E$. Linearizing this nonlinear $\chi(N)$ around the transparency density N_{tr}, one obtains

$$\begin{aligned} \chi(N) &= \left(\frac{\partial \chi'}{\partial N} + i\frac{\partial \chi''}{\partial N}\right)(N - N_{tr}) + ... \\ &\equiv -iG_L(1 - i\alpha)/K, \end{aligned} \tag{10}$$

where $G_L = -\frac{\partial \chi''}{\partial N}(N - N_{tr})$ is the linear gain and $\alpha = \frac{\partial \chi'}{\partial N}/\frac{\partial \chi''}{\partial N}$ is the linewidth enhancement factor introduced by Haug and Haken[12] (see, also[31]). From the above definitions and from (1-3) we then obtain:

$$\frac{\partial E}{\partial z} + \frac{n_g}{c}\frac{\partial E}{\partial t} = \frac{\Gamma}{2} G_L(1 - i\alpha)E \tag{11}$$

$$\frac{dN}{dt} = -\gamma_N N + \frac{\eta J}{ew} + \frac{\epsilon_0 c n_b G_L}{2\hbar\omega_c}|E|^2, \tag{12}$$

where the parameters η, J, e, w are respectively, the quantum efficiency, pumping current, electron charge, and active region thickness. The relation between the pumping current density J and the microscopic pumping expressions can be found, for example, in reference.[2]

The advantage of using this model is that it is simple and that it captures some of the important features of semiconductor lasers. The disadvantages are also obvious. The linearized gain model requires that the carrier density within the active semiconductor must be very close to the given density (very often, the transparency density). This assumption fails on several occasions: In a typical semiconductor laser, the lateral carrier distribution is determined by the shape of the pumping stripe and carrier diffusion. The carrier density at the lateral edges of the device changes between around threshold to zero within some finite region (see Fig.4).

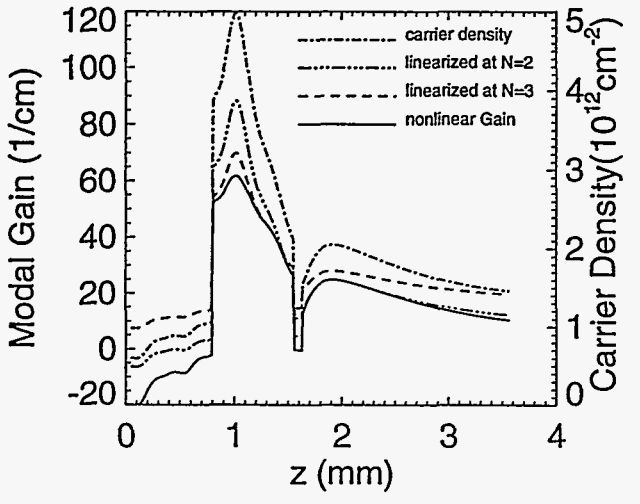

Figure 3. On-axis density variation and the corresponding gain profiles using different gain models along the MOPA structure[20,34].

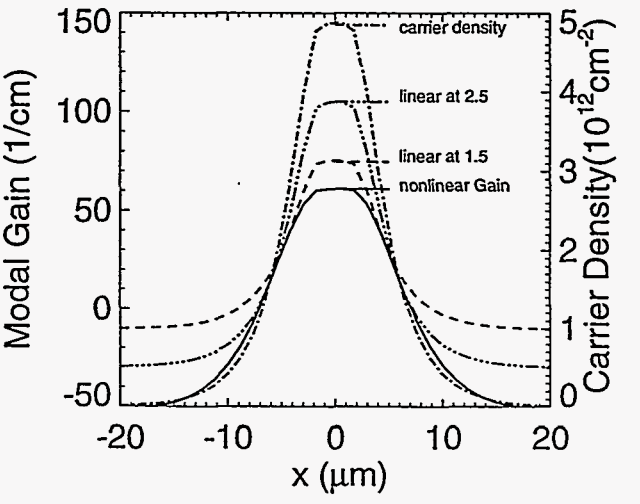

Figure 4. Density variation and the corresponding gain profiles using different gain models lateral to the DBR laser structure in the MOPA[20,34].

The active medium changes from an amplifier to an absorber, depending on the local carrier density. Another example is a DBR laser where the same active material is used for the pumped region as that underneath the DBR sections. Usually DBR sections act as absorbers with quite strong variation of the carrier density along the DBR sections. The strength of the absorption is very crucial to the overall DBR laser performance. In some of the high power devices, such as the DBR-Master Oscillator integrated with a Power Amplifier (MOPA), the longitudinal and lateral density variation is very significant.[34] Fig.3 and Fig.4 show the carrier distribution along and across such a MOPA device together with the corresponding gain profiles. We also plot the linearized gain at different densities and the actual nonlinear gain. Obviously all these situations cannot be taken into account by a simple linearized gain.

3.2. Rate equations with nonlinear gain

The shortcoming of the linear gain model can be overcome by keeping the actual nonlinear dependence of gain ($G(N)$) and index change ($\delta n(N)$) on carrier density.[29] Similar to the derivation of equations (11) and (12), we obtain

$$\frac{\partial E}{\partial z}+\frac{n_g}{c}\frac{\partial E}{\partial t} = \frac{\Gamma}{2}\left(G(N)+i\frac{2\omega_c}{c}\delta n(N)\right)E \tag{13}$$

$$\frac{dN}{dt} = -\gamma_N N+\frac{\eta J}{ew}+\frac{\epsilon_0 c n_b G(N)}{2\hbar\omega_c}|E|^2, \tag{14}$$

For a given laser structure, a microscopic calculation is performed to obtain the actual nonlinear carrier density dependence of the gain and index change at the peak gain frequency. This dependence is then tabulated as lookup tables to be used in the actual simulation of equations (13) and (14). A detailed comparison between the nonlinear and linear gain models is made in.[29]

3.3. Gain and refractive index dispersion

There is, however, another serious problem that cannot be overcome by either a linear or nonlinear gain model. The gain and refractive index dispersion (the frequency dependence) is not considered in either of these approaches. This means that all the longitudinal and transverse modes experience the same gain or index change. In the case of pulse propagation, different frequency components of the pulse undergo the same amplification. This is certainly a poor representation of what happens in a semiconductor laser or amplifier. The gain dispersion, no matter how small, is very critical in influencing the long time dynamics of semiconductor lasers. The index dispersion which results in a frequency dependent α factor is also important for semiconductor laser modeling. The absence of the gain discrimination leads to the artificial instabilities that are very easily mistaken for numerical instabilities.[33]

The microscopic theory as represented by the semiconductor Bloch equations (SBEs) contains all the features mentioned above. However, due to the widely varying time scales involved and the complexity of the set of equations, it is almost impossible to solve the SBEs on the nanosecond time scale and resolve, at the same time, the transverse and longitudinal space dimensions.

From the above discussion, it is clear that a model is needed that contains the actual gain and index spectra and their carrier density dependence. Such a model has recently been constructed[24] for the free-carrier theory. As we have shown in this section, many-body interactions are very important in modifying gain and refractive index spectra and therefore should be incorporated into theory.

4. EFFECTIVE BLOCH EQUATIONS

Our approach[30] is based on the parameterization of the gain and refractive index spectra. We assume that the susceptibility function $\chi(\omega, N)$ for a given laser structure is known either from the above microscopic calculation, or from an experimental measurement. We assume that this function can be well approximated, in general, by a superposition of several (M) Lorentzian oscillators:

$$\chi(N,\omega) \approx \chi_0(N) + \sum_l^M \frac{A_l(N)}{i\Gamma_l(N) + (\delta_0 + \omega - \delta_l(N))} \equiv \chi_0(N) + \sum_l^M \chi_l(\omega, N), \tag{15}$$

where we also include a "background" contribution $\chi_0(N)$ which is frequency independent. In (15) we use a detuning parameter: $\delta_0 = \omega_c - E_g/\hbar$. Note that we allow the density dependence of the "parameters" $A_l(N)$, $\Gamma_l(N)$, and $\delta_l(N)$ for the individual Lorentzian oscillators. The density dependence of the gain and refractive index spectra are now taken into account by these density dependent parameters. In general we expect to approximate the susceptibility function quite well using only a few such oscillators. For many applications, however, it suffices to have only one such Lorentzian oscillator plus the "background" absorption and index. An example for this approximation is shown in Fig.5 where gain and index spectra for bulk GaAs, calculated from the microscopic theory for three different densities, are plotted (solid lines) together with the spectra of the approximations using (15) (dashed lines).

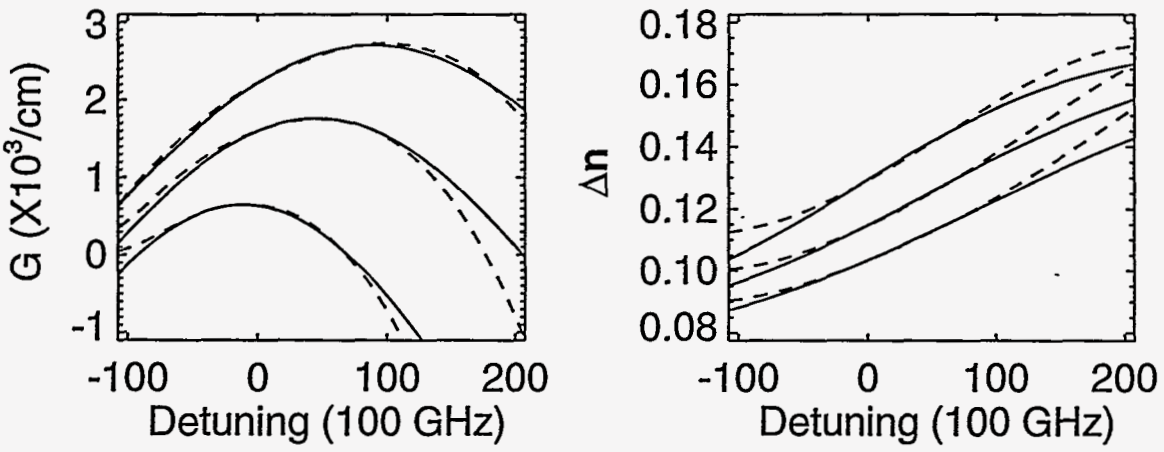

Figure 5. Gain (left) and index (right) spectra for carrier density of 2, 3, and 4 $\times 10^{18}/cm^3$, respectively. Solid lines are fitted with a single Lorentzian, while dashed lines are the results computed numerically from the SBEs.

Once we have the parameterized Lorentzian oscillators, we can easily write down the corresponding polarization in the Fourier representation.

$$\begin{aligned} \tilde{P}_0 &= \epsilon_0\epsilon_b\chi_0(N)\tilde{E}(\omega), \\ \tilde{P}_j(\omega) &= \epsilon_0\epsilon_b\tilde{\chi}_j(N,\omega)\tilde{E}(\omega) = \frac{\epsilon_0\epsilon_b A_j(N)\tilde{E}(\omega)}{i\Gamma_j(N) + \delta_0 + \omega - \delta_j(N)}, \quad (j = 1, 2\ldots) \end{aligned} \tag{16}$$

The total polarization in real space is given by:

$$\frac{1}{V}\sum_k \mu_k p_k = P_0 + P_1 + P_2 + \ldots \tag{17}$$

If we perform the inverse Fourier transform of equation (16), we obtain

$$\frac{dP_j(t)}{dt} = \{-\Gamma_j(N) + i[\delta_0 - \delta_j(N)]\}P_j(t) - i\epsilon_0\epsilon_b A_j(N)E(t), \quad (j = 1, 2, \ldots) \tag{18}$$

while for $(j = 0)$ we have $P_0(N) = \epsilon_0\epsilon_b\chi_0(N)E(t)$, because no frequency dependence of $\chi_0(N)$ is assumed. It is important to note that, in performing the Fourier transformation, we have treated density-dependent functions $\Gamma_j(N)$, $\delta_j(N)$, $A_j(N)$, and $\chi_0(N)$ as if they were independent of time. In fact this is not the case, because these functions depend on a time-varying density. However, this is still a good approximation as long as the carrier density changes much more slowly compared to the inverse gain bandwidth. This is obviously true in a typical laser. For very strong and short pulses, this assumption needs to be reexamined.

Once we have the equations for P_j, we can sum over the $k-$ resolved density equations (3)of the SBEs[1,2] to obtain the equation for the total carrier density.

$$\frac{dN}{dt} = -\gamma_N N + \frac{\eta J}{ew} + \frac{i}{4\hbar}\left[(P_0 + P_1 + \ldots)^* E - (P_0 + P_1 + \ldots)E^*\right]. \tag{19}$$

Equation (1) for the laser field amplitude is now written as

$$\frac{\partial E}{\partial z} + \frac{n_g}{c}\frac{\partial E}{\partial t} = \frac{iK\Gamma}{2\epsilon_0\epsilon_b}(P_0 + P_1 + \ldots), \tag{20}$$

Equations (18,19,20) form the basic set of equations for our model. These equations contain density dependent parameters which must be obtained from the independent calculation of gain and index spectra, or from experimental measurements. If the lateral variation is to be resolved, we can add a carrier diffusion term in (19) and a diffraction term in (20).

5. COMPARISON BETWEEN EBEs AND SBEs

To test the validity of the EBEs (18-20), we consider pulse propagation in a bulk GaAs semiconductor amplifier by solving both the SBEs and the EBEs. In our solution of the SBEs, the scattering terms are treated using scattering rate approximation, both for carrier-carrier and for carrier-phonon scatterings. First we consider propagation of an initially strong pulse of amplitude 6 meV. The input pulse is sech-shaped with FWHM of 20 ps. Fig.6(a) shows the pulse profiles at selected propagation distances into the medium. The corresponding plasma temperature rise is shown in Fig.6(b). In spite of the plasma temperature rise of about 10K and in spite of the fact that no temperature effect is considered in the EBE model, the two profiles agree very well with each other. The more stringent test of the model is for the shorter pulse propagation. Fig.7 shows the last portion of the propagation of an initially short pulse of 2 ps duration. The initial amplitude is 0.1 meV. We see that, with propagation into the medium, the two profiles start to diverge with the one simulated by the SBEs giving lower profile than the one by EBEs.

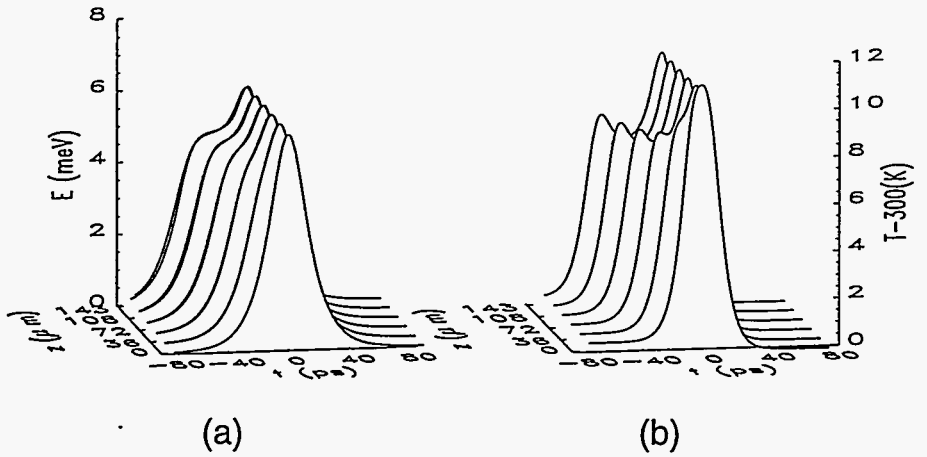

Figure 6. (a) Pulse profiles using the SBEs and the EBEs. (b) The corresponding temperature profile as predicted by the SBEs.

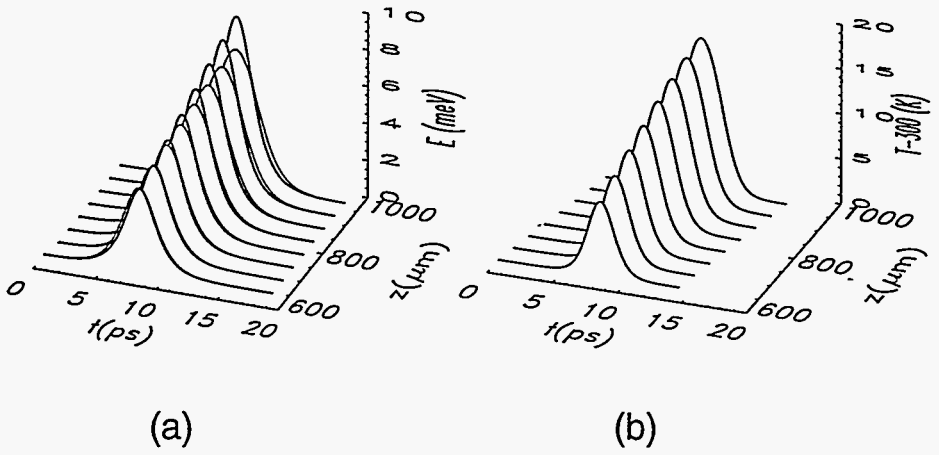

Figure 7. (a) Pulse profiles using the SBEs(lower one) and the EBEs(higher one). (b) The corresponding temperature profile as predicted by the SBEs.

In Fig.7(b), we see that the plasma temperature rise in this case is larger than in Fig.7(b). This more significant plasma heating leads to a stronger saturation of the gain, and therefore less amplification of the pulse. From this comparison, we conclude that for the pulse width of tens of picoseconds, the EBE model gives good agreement. When the pulse becomes shorter, the plasma heating plays a more important role. Since our model does not include plasma heating, it fails for the propagation of pulses of a few picosecond duration. It is worthwhile to mention that our main intended application area is modeling laser dynamics, in which case, the time scales involved are usually much longer than a few picoseconds, or the amplitude of the electric field is much smaller. In these cases, we expect that this model to work well. Obviously, if we can generalize the present model to include plasma heating, the range of validity could be further extended.

6. SUMMARY

We have shown in the previous sections of this paper why it is necessary to include the nonlinear carrier density dependence and dispersion of the gain and refractive index for semiconductor laser modeling. Our main purpose is then to incorporate these dependences into a set of modeling equations. Because many-body interactions are very important in determining the spectral shape and amplitude of the gain and refractive index change, it is natural that such a systematic model should take Coulomb interactions into account. Our systematic, bottom-up construction of the effective Bloch equations also takes the material and structure parameters into account. Because the approach is based on the approximation of the gain and refractive index by Lorentzian oscillators, it could be equally well applied to experimentally measured data. A summary of our approach and the detailed procedure are shown in Fig.8. We think that the flexibility of this comprehensive model will allow more quantitative investigation of the space-time dynamics of broad-area semiconductor lasers, complex laser arrays, and other more complex laser structures. Currently we are working on the inclusion of the temperature effects in the same fashion.

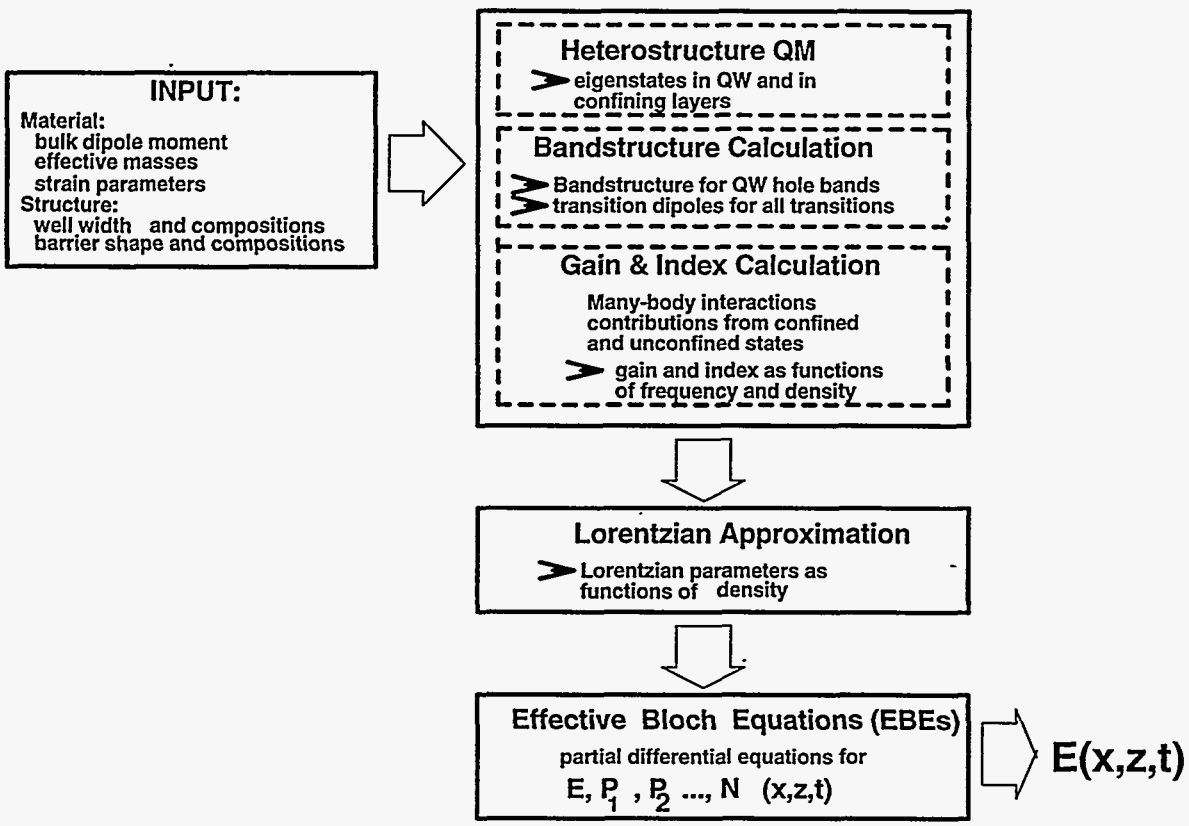

Figure 8. Summary schemes used in our approach.

ACKNOWLEDGEMENTS

The work at Arizona is sponsored by the Air Force Office of Scientific Research, Air Force Materiel Command, USAF, under contract AFSOR F 49620-94-1-0144 DEF. The U.S. Government is authorized to reproduce and distribute reprints for Governmental purposes notwithstanding any copyright notation thereon. The work at Sandia is supported by the U.S. Department of Energy through contract No. DE-AC04-94AL8500. Sandia is a multiprogram laboratory operated by Sandia Coporation, A Lockheed Martin company, for the United States Department of Energy. The Marburg group is financially supported by the Deutschforschungsgemeinschaft (DFG) and the Leibniz Prize.

REFERENCES

1. H.Haug and S.W. Koch, *Quantum Theory of the optical and electronic properties of semiconductors*, 2nd. (World Scientific, Singapore, 1993)
2. W. W. Chow, S. W. Koch, and M. Sargent, *Semiconductor Laser Physics*, Springer, Heidelberg, Berlin, 1994
3. A. Knorr, R. Binder, M. Lindberg and S.W. Koch, Theoretical study of resonant ultrashort-pulse propagation in semiconductors, Phys. Rev. A 46, pp. 7179-7186(1992)
4. R.A. Indik, J.V. Moloney, R. Binder, W.W. Chow, A. Knorr, S.W. Koch, Many-body effects in the propagation of short pulses in a semiconductor amplifier, SPIE-Proceedings, Vol. 2399, pp. 650-659(1995)
5. A.Knorr, S.Hughes, T.Stroucken, and S.W. Koch, Theory of ultrafast spatio-temporal dynamics in semiconductor heterostructures Chemical Physics 210, 27 (1996)
6. M. Hoffmann, M. Koch, J. Feldmann, W. Elsäßer, E.O. Göbel, W.W. Chow, adn S.W. Koch, "Picosecond gain dynamics of an actively mode-locked external- cavity laser diode", IEEE J. Quant. Electron. QE-30 , pp. 1756-1762(1994).
7. R. Jin, D. Boggavarapu, G. Khitrova, H.M. Gibbs, Y.Z. Hu, S.W. Koch, and N. Peyghambarian, " Linewidth broadening factor of a microcavity semiconductor laser", Appl. Phys. Lett., 61, pp. 1883-1885(1992)
8. Y.H. Lee, A. Chavez-Pirson, S.W. Koch, H.M. Gibbs, S.H. Park, J. Morhange, A. Jeffery, N. Peyghambarian, L. Banyai, A.C. Gossard, and W. Wiegmann, "Room-temperature optical nonlinearities in GaAs", Phys. Rev. Lett., 57, pp. 2446-2449(1986)
9. W.W. Chow, S.W. Corzine, D.B. Young, and L.A. Coldren, " Many body effects in the temperature dependence of threshold in a vertical-cavity surface-emitting laser", Appl. Phys. Lett 66, pp. 2460-2462(1995).
10. C.Z. Ning, W.W. Chow, D.J. Bossert, R.A. Indik, J.V. Moloney, Influences of unconfined states on the optical properties of quantum well structures, IEEE J. Spectial Topics in Quant. Electron., Semiconductor Lasers, June 1997
11. E. Haken and H.Haken, Zur Theorie des Halbleiter Lasers, Z. Phys., 176, pp. 421-428(1963)
12. H. Haug and H. Haken, "Theory of noise in semiconductor laser emission", Z.Phys. 204,pp. 262-275 (1967)
13. H.Haug, Phys. Rev. 184, pp. 338- (1969)
14. P.D. Dapkus, N. Holonyak Jr., J.A. Rosi, F.V. Willianms, and D.A. High, J. Appl. Phys., 40, p. 3300, (1969)
15. M. Lindberg and S.W. Koch, "Effective Bloch equations for semiconductors", Phys. Rev. 38 B pp. 3342-3350(1988)
16. H. Haug and S.W. Koch, Semiconductor laser theory with many-body effects, Phys. Rev. A, 39, pp. 1887-1898, (1989)
17. O.Hess, S.W. Koch, and J.V. Moloney, "Filamentation and Beam propagation in Broad-area semiconductor lasers", IEEE J. Quant. Electron., 31, pp. 35-43(1995).
18. J.V. Moloney, R.A. Indik, and C.Z. Ning," Full space-time simulation of high-brightness semiconductor lasers", (to be published)
19. A.Larsson, M.Mittlestein, Y. Arakawa, and A. Yariv, "High efficiency broad-area single quantum well lasers with narrow single-lobed far-field patterns prepared by molecular beam epitaxy", Electon. Lett., 22, pp. 79-81(1986)
20. D.F. Welch, R. Parke, D. Mehuys, A. Hardy, R. Lang, S. O'Brien, and S. Scifres, "1.1W CW, diffraction-limited operation of a monolithically-integrated flared amplifier master oscillator power amplifier", Electron. Lett., 26, pp. 2011-2012(1991)
21. D.J. Bossert and D. Gallant, "Gain, Refractive index and α-parameter in *InGaAs/GaAs* SQW broad-area lasers", IEEE Photon. Techn. Letts., 8, pp. 322-324(1996)
22. M.S. Hybertsen, R.F. Kazarinov, G.A. Baraf, D.A. Ackerman, G.E. Shtengel, P.A. Mortan, T. Tanbun-Ek, and R.A. Logan, in " Physics and Simulation of Optoelectronic Devices III ", M. Osinski, W.W. Chow, Editors, Proc.-SPIE 2399, pp.132-145(1995).
23. J. Nagel, S. Hersee, M. Krakowski, T. Weil, and C. Weisbuch, Theoretical current of single quantum well lasers: The role of the confining lasers, Appl. Phys. Lett., 49, pp.1325-1327(1986)
24. J. Yao, G.P. Agrawal, P. Gallion, and C. Bowden, Opt. Commun. 119,pp. 246-255(1995)
25. H. Statz and G.A. de Mars: in Quantum Electronics, ed. by C.H.Towns (Columbia, New York, 1960), pp. 503-537